Article

Mechanical Biocompatibility, Osteogenic Activity, and Antibacterial Efficacy of Calcium Silicate−Zirconia Biocomposites

Shinn-Jyh Ding,* Ying-Hung Chu, and Pei-Tung Chen

Read Online

ACCESS | Metrics & More | Article Recommendations

ABSTRACT: Zirconia ceramics with high mechanical properties have been used as a load-bearing implant in the dental and orthopedic surgery. However, poor bone bonding properties and high elastic modulus remain a challenge. Calcium silicate (CaSi)-based ceramic can foster osteoblast adhesion, growth, and differentiation and facilitate bone ingrowth. This study was to prepare CaSi-ZrO_2 composites and evaluate their mechanical properties, long-term stability, in vitro osteogenic activity, and antibacterial ability. The *Escherichia coli* (*E. coli*) and *Staphylococcus aureus* (*S. aureus*) bacteria and human mesenchymal stem cells (hMSCs) were used to evaluate the antibacterial and osteogenic activities of implants in vitro, respectively. Results indicated that the three-point bending strength of ZrO_2 was 486 MPa and Young's modulus was 128 GPa, which were much higher than those of the cortical bone. In contrast, the bending strength and modulus of 20% (201 MPa and 48 GPa, respectively) and 30% CaSi (126 MPa and 20 GPa, respectively) composites were close to the reported strength and modulus of the cortical bone. As expected, higher CaSi content implants significantly enhanced cell growth, differentiation, and mineralization of hMSCs. It is interesting to note the induction ability of CaSi in osteogenic differentiation of hMSCs even when cultured in the absence of an osteogenic differentiation medium. The composite with the higher CaSi contents exhibited the greater bacteriostatic effect against *E. coli* and *S. aureus*. In conclusion, the addition of 20 wt % CaSi can effectively improve the mechanical biocompatibility, osteogenesis, and antibacterial activity of ZrO_2 ceramics, which may be a potential choice for load-bearing applications.
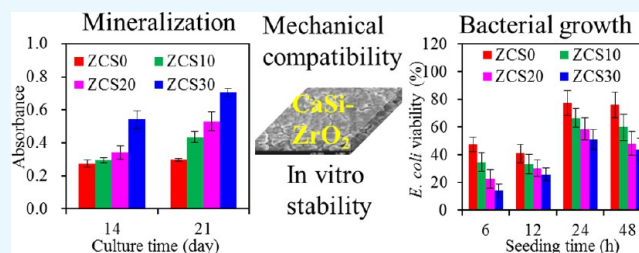
1. INTRODUCTION

Biocompatible, wear-resistant, and esthetic ceramics have been widely used in load-bearing biomedical applications, including total hip and knee replacements and dental restorations.[1−5] Among ceramics, zirconia (such as yttria-stabilized tetragonal zirconia polycrystals; Y-TZP) is one of the most important ceramic materials because of high mechanical properties and chemical stability in vivo.[2,6] In addition, zirconia not only lacks the cytotoxicity or mutagenic effects but also shows osseointegration and low inflammatory infiltration in the gingival tissue.[7,8] Comparative studies of in vitro biocompatibility and in vivo osseointegration of ZrO_2 and titanium implants show similar behaviors on the implant surface and the bone−implant contact.[9] However, in a 7 year follow-up of retrospective clinical study, 36 out of 161 zirconia implants (22.4%) are lost due to the failures and fractures.[10] Therefore, new load-bearing implant systems have to be developed to achieve advanced performance. In order to enhance the osteogenesis of the zirconia implant, surface modification techniques have been designed to induce tissue growth. Cho et al. coated zirconia surfaces with hydroxyapatite (HA) by the aerosol deposition method to improve in vitro osteogenic activity.[11] Zhang et al. used a mesoporous bioactive glass coating to increase the bioactivity of Ce-TZP/Al_2O_3 ceramics.[12]

Ideally, synthetic load-bearing implants should mimic natural bone tissues in mechanical and osteogenic properties to facilitate the bone healing. In terms of mechanical biocompatibility, the elastic modulus of the implant material needs to match that of the bone tissue to prevent "stress shielding".[13] It is well known that the elastic modulus of ZrO_2 (200 GPa) is much higher than that of the cortical bone (7−30 GPa).[14] The higher Young's modulus of the implant makes it difficult to transfer uniform stress to the surrounding bone tissue, thereby resulting in stress shielding that causes bone loss/fractures.[2,15] Kohal et al. found that the peri-implant bone loss value after 1 year follow-up of one-piece zirconia oral implants was considerably higher than the conventional two-piece titanium implants.[16] Sumner and Gatahte[13] and Geetha

Table 1. Mechanical Properties of the ZrO_2-Based Composites as a Function of the CaSi Content[a]

sample code	density (g/cm³)	three-point bending		biaxial strength (MPa)	hardness (Hv)
		strength (MPa)	Young's modulus (GPa)		
ZCS0	5.7 ± 0.2[a]	486 ± 43[a]	128 ± 21[a]	1164 ± 102[a]	1406 ± 41[a]
ZCS10	4.7 ± 0.1[b]	259 ± 29[b]	78 ± 4[b]	631 ± 57[b]	1012 ± 86[b]
ZCS20	4.1 ± 0.1[c]	201 ± 12[b]	48 ± 4[c]	484 ± 29[c]	708 ± 93[c]
ZCS30	3.8 ± 0.1[d]	126 ± 8[c]	20 ± 4[d]	325 ± 23[d]	622 ± 73[c]

[a]Mean values followed by different superscript letters were significantly different ($p < 0.05$) according to Scheffé post-hoc multiple comparisons.

et al.[17] suggested that matching the modulus of the implant to that of the host bone tissue can avoid loosening of implants and extend device lifetime. In theory, stress-shielding effects can be modulated by altering the implant properties. However, a literature search indicates that few articles address the mechanical biocompatibility of zirconia-based composites with bone tissue, and most articles relate to biocompatibility.[18,19] On the other hand, implant-associated infections have been a serious complication in dentistry and orthopedics due to the resorption of the peri-implant bone, which may eventually result in the removal of the implant.[20] Bacterial adhesion always plays an initial role in the development of bacterial colonies. Poor microbial antiadhesive ability of the material will cause implantation and repair failure.[21] Egawa et al. reported that the periodontopathic bacteria adhered to Y-TZP similarly to titanium implants,[22] indicating considerable peri-implantitis. The presence of bacteria on the implant surface will complicate the process of osseointegration and may even fails to osseointegrate.[23,24] Prevention of bacterial colonization and formation of a bacterial biofilm on implant surfaces are an increasing demand.

The approach aimed at improving the mechanical biocompatibility and biological properties of zirconia implants to develop new composite ceramics by adding bioactive materials to the zirconia matrix. Calcium silicate (CaSi)-based bioceramics have been used for bone tissue repair and regeneration. In vitro cell culture studies have shown that CaSi-based materials can support the attachment, proliferation, and differentiation of human bone mesenchymal stem cells[25,26] and human pulp cells.[24] More importantly, the newly formed bone tissue can grow on the surface of CaSi in rabbit calvarial defect[27] and minipig mandibular alveolar bone defect models.[28] It is worth mentioning that CaSi-based materials have shown antibacterial activity against a variety of bacterial strains.[29−31] Therefore, it is expected that CaSi can be effectively used as a reinforcing additive because of its good osteogenesis and antibacterial activity. More importantly, the addition of low modulus CaSi[32] may reduce the high modulus of tough ZrO_2 due to the composition effects, which alleviated the stress-shielding effect. In this study, we used a simple direct mixing method to prepare CaSi-ZrO_2 composites. The mechanical properties, long-term in vitro degradation in an acidic environment, osteogenic activity, and antibacterial ability of the composite implant were systematically evaluated. Regarding the mechanical test, according to the ISO 6872 standard (Dentistry—Ceramic Materials), the uniaxial (three-point bending) and biaxial (piston-on-three-ball) flexural strengths of the materials were checked because they may be subjected to different axial impacts in clinical practice.[33] Two different bacterial species (including Gram-negative *Escherichia coli* (*E. coli*) and Gram-positive *Staphylococcus aureus* (*S. aureus*)) represented by different bacterial types were used to explore the antibacterial efficacy of composite materials. The biological function of the material was examined using human mesenchymal stem cells (hMSCs).

2. MATERIALS AND METHODS

2.1. Preparation of Composites. Details of the procedure for preparing sol−gel-derived CaSi powders (Ca/Si = 1 in molar ratio) have been described elsewhere.[15] Tetraethyl orthosilicate ($Si(OC_2H_5)_4$) (Sigma-Aldrich, St. Louis, MO, USA) and calcium nitrate ($Ca(NO_3)_2·4H_2O$) (Showa, Tokyo, Japan) were used as precursors for SiO_2 and CaO, respectively. After mixing, aging, and drying, the powder was sintered at 800 °C in air and then ball-milled in ethanol using a Retsch S 100 centrifugal ball mill (Hann, Germany) for 24 h. The fine CaSi powder was added to 3 mol % Y_2O_3-stabilized ZrO_2 powder (TZ-3YB-E; Tosoh, Tokyo, Japan) at 10, 20, and 30 wt % using a Thinky ARE-250 mixer (Tokyo, Japan) at 1000 rpm for 5 min. The sample code "ZCS10" represented a mixture containing 10 wt % CaSi, as shown in Table 1. By uniaxial pressing at 100 MPa for 2 min, the mixtures were compacted into rectangular bars of 24 mm × 4 mm × 4 mm or cylindrical pellets with a diameter of 15 mm. Afterward, the green body was sintered at 1350 °C at a heating rate of 10 °C/min for 3 h, and then it was cooled to room temperature. Each sintered sample was polished with a 1 μm diamond suspension (Buehler, Lake Bluff, IL, USA) for assays.

2.2. Morphology, Phase Composition, and Density. The raw powders and polished surfaces of the sintered blocks were coated with gold using a JFC-1600 coater (JEOL, Tokyo, Japan), and the morphologies were then observed using a field-emission scanning electron microscope (SEM; JEOL JSM-7800F, Tokyo, Japan) at a lower secondary electron image (LEI) mode. The chemical composition of the material was determined by energy-dispersive X-ray spectroscopy (EDS). Phase analysis was performed using an X-ray diffractometry instrument (XRD; Bruker D8 SSS, Karlsruhe, Germany) with Ni-filtered Cu Kα radiation operating at 40 kV, 100 mA, and a scanning speed of 0.5°/min. The apparent density was measured by a liquid displacement technique.[29]

2.3. Mechanical Properties. *2.3.1. Three-Point Bending Test.* The three-point bending test was conducted on a static mechanical testing machine AG-1000E (Shimadzu, Kyoto, Japan) with a 10 kN load cell with a crosshead speed of 1 mm/min. After sintering at 1350 °C, the final size of the rectangular sample was about 18 mm × 3 mm × 3 mm. Prior to the bending strength test, the dimensions of the samples were measured with a digital micrometer (Absolute Digimatic Caliper, Mitutoyo, Tokyo, Japan) with an accuracy of 0.01 mm. The span length was 16 mm. As the sample was bent, the ultimate bending strength (σ_b) and Young's bending modulus (E_b) were calculated as follows

$$\sigma_b = \frac{3F_{max}L}{2wt^2} \text{ and } E_b = \frac{L^3}{4wt^3}\frac{\Delta F}{\Delta l}$$

where F_{max} is the maximum load (N), L is the support span (mm), w and t are the width (mm) and thickness (mm) of the sample, respectively, and $\Delta F/\Delta l$ is the slope of the initial linear elastic portion of the load−deflection curve (N/mm). The data provided by each group were the mean of 20 independent measurements.

2.3.2. Biaxial Flexural Test. To examine biaxial flexural strength, each cylindrical sample ($n = 20$ per group) was placed centrally on three hardened steel balls (a diameter of 3 mm, positioned 120° apart on a support circle with a diameter of 10 mm).[34] The polished surface of the sample was the tension side, while the unpolished surface was loaded with a flat punch (1.2 mm in diameter). The biaxial flexural strength was obtained using an AG-1000E where the load was applied at a constant speed of 1 mm/min until fracture occurred. The load that led to the initial separation of samples was obtained in newton (N) and converted to MPa using the following equation

$$S = -0.2387P(X - Y)/d^2$$

where "S" is the maximum center tensile stress (MPa) and "P" is the total load causing fracture (N)

$$X = (1 + \nu)\text{In}(r_2/r_3)^2 + [(1 - \nu)/2](r_2/r_3)^2$$

$$Y = (1 + \nu)[1 + \text{In}(r_1/r_3)^2] + (1 - \nu)(r_1/r_3)^2$$

where ν is the Poisson ratio. If Poisson's ratio of the ceramic is known, a value of 0.25 is used; r_1 is the radius of the support circle (mm); r_2 is the radius of the loaded area (mm); r_3 is the sample radius (mm); and d is the sample thickness at fracture origin (mm).

2.3.3. Hardness Test. A digital microhardness tester (HMV-2000, Shimadzu, Kyoto, Japan) with a four-sided diamond pyramid was used to evaluate the microhardness of various cylindrical samples. Vickers microhardness (Hv) was obtained from the equation $1.854P/d^2$, where P is the load (N) and d is the average diagonal length (mm) of the impression. A load of 19.6 N for 15 s in air was used. The average was determined from 30 collections using 10 samples.

2.3.4. Fatigue Test. The three-point bending mode was used to examine the fatigue behavior of the specimen. A fatigue cyclic loading lower than the static three-point bending strength was applied with a stress ratio of $S_{min}/S_{max} = 0.1$ at 5 Hz until fracture was achieved using a Shimadzu servopulser 48000 system (Kyoto, Japan), where S_{max} is the maximum three-point stress and S_{min} is the minimum three-point stress. The three-point bending test generates compressive stress on the concave side of the sample to which an external force is applied and tensile stress on the convex side at the two support pins.[35] The three-point bending test generates compressive stress on the concave surface of the specimen and tensile stress on the convex surface. The number of cycles to failure under cyclic compression or tensile conditions was promptly recorded as the sample ruptured. Twelve samples of each group were examined.

2.4. In Vitro Degradation. Simulated body fluid (SBF) solution is usually used as the supporting solution for the in vitro degradation test. In order to simulate the continuous circulation of physiological fluids in the body, continuous exchange of SBF (dynamic condition) may be a more effective assay, which can predict in vitro degradation more accurately than a static assay (lack of SBF exchange).[36] The feeding rate of the peristaltic pump was 1 mL/min. Since a fresh solution was provided, the exchange of the solution could keep the ionic concentration and pH of the SBF almost constant. The SBF solution was buffered to pH 5.0 with hydrochloric acid and tris(hydroxymethyl)aminomethane, which the pH value can simulate the acidic environment caused by bone infections. The ratio of the sample surface to the SBF volume was 0.1 cm^{-1}. After soaking for specific time (1, 3, and 6 months), 20 samples were taken from the vial to determine biaxial strength and microhardness. The other samples were dried in an oven at 60 °C to analyze weight loss, porosity, phase composition, and morphology. To measure weight loss, a four-digit balance (AE 240S, Mettler-Toledo AG, Greifensee, Switzerland) was used to weigh the dried samples until a constant weight was reached before (day 0) and after soaking. Twelve repeated samples were examined for each group at each time point. The porosity of the samples was evaluated by the Archimedes' gravimetric method.[36]

2.5. hMSC Responses. *2.5.1. Cell Growth.* The cell response to the samples was assessed by incubation with hMSCs (Cell Engineering Technologies, Coralville, IA, USA) at passages 3−6. Prior to cell incubation, samples (1 mm in thickness and 12 mm in diameter) were sterilized using 75% ethanol and then exposed to ultraviolet (UV) light for 2 h. hMSCs were seeded at a density of 10^4 cells/well on sterilized samples in 24-well plates. The cell growth medium was Dulbecco's modified Eagle's medium (DMEM; Gibco, Langley, OK, USA) containing 10% fetal bovine serum (FBS) (Gibco) and 1% penicillin/streptomycin solution (Gibco) in 5% CO_2 at 37 °C, which was changed every 2 days. After being cultured for 1, 3, and 7 days, the cell growth was measured by the MTT (3-(4,5-dimethylthiazol-2-yl)-2,5-diphenyltetrazolium bromide; Sigma-Aldrich) assay, which was detected using a BioTek Epoch spectrophotometer (Winooski, VT, USA) at 563 nm, following a previous protocol.[28] The data expressed in absorbance were the average of three independent measurements.

2.5.2. ALP Activity. Alkaline phosphatase (ALP) activity of hMSCs, an early marker of osteogenesis, was examined at a density of 5×10^3 cells/well after 7 and 14 days of incubation. The growth medium was replaced with the induction medium to guide osteogenic differentiation, which consisted of the growth medium supplemented with 10 nM dexamethasone, 10 mM β-glycerophosphate, and 0.05 mM ascorbic acid. The growth medium alone was also used for comparison purposes to verify the osteogenic efficacy of CaSi. ALP activity was measured using the TRACP & ALP assay kit (Takara, Shiga, Japan), and the detailed assay was described elsewhere.[34] Three separate experiments were performed.

2.5.3. Mineralization. Alizarin red S staining was utilized to analyze mineralized matrix synthesis of hMSCs after being cultured for 14 and 21 days. The cells were washed with phosphate buffer solution (PBS, pH 7.4), fixed in 4% paraformaldehyde (Sigma-Aldrich) for 10 min, and then stained in 0.5% alizarin red S (Sigma-Aldrich) in PBS for 10 min. After being washed with PBS, the stained cells were observed using an optical microscope (BH2-UMA; Olympus, Tokyo, Japan). Further, the calcium mineral precipitate was destained using 10% cetylpyridinium chloride (Sigma-Aldrich) in PBS for 30 min in order to quantify matrix mineralization. The absorbance of alizarin red S extract was assayed using a

BioTek Epoch microplate reader at 562 nm. Three runs per group were performed.

2.6. Antibacterial Activity. *2.6.1. Bacterial Viability.* E. coli (ATCC 8739 Hsinchu, Taiwan) and *S. aureus* (ATCC 25923, Hsinchu, Taiwan) were used to evaluate the antibacterial activity (or microbial antiadhesive activity) of a cylindrical sample with a diameter of 12 mm. Prior to seeding bacteria, all samples were sterilized with 75% ethanol and then exposed to UV light for 2 h. After washing three times with PBS, the sample was placed in a 24-well culture plate, and 1 mL of bacteria was seeded at a density of 10^7 CFU/mL in Bacto tryptic soy broth (Beckton Dickinson, Sparks, MD, USA) for 6, 12, 24, and 48 h. Subsequently, the samples were checked for antibacterial activity by the alamarBlue (Invitrogen, Grand Island, NY, USA) assay.[24] The absorbance results were recorded for eight independent measurements using a BioTek Epoch spectrophotometer at 570 nm with a reference wavelength of 600 nm. Viability data (%) were obtained by normalizing the absorbance with respect to the culture broth without implant samples.

2.6.2. Bacterial Colony. To further observe the number of bacterial colonies, 24 h after the inoculation, the samples were washed three times with PBS and fixed in 4% paraformaldehyde (Sigma-Aldrich) for 20 min. After that, samples were dehydrated using a graded ethanol series for 20 min at each concentration, then mounted on a stub, coated with a gold layer, and then viewed by SEM.

2.7. Statistical Analysis. One-way analysis of variance (ANOVA) and post-hoc Scheffé's test were used to examine the significant difference between the means in the measurement data using SPSS 14.0 software for Windows (SPSS Inc., Chicago, IL, USA). The results were considered statistically different at a *p*-value of less than 0.05.

3. RESULTS

3.1. Morphology of Powder. Figure 1 shows SEM images of the ZrO_2 and CaSi raw powders used in this study. The
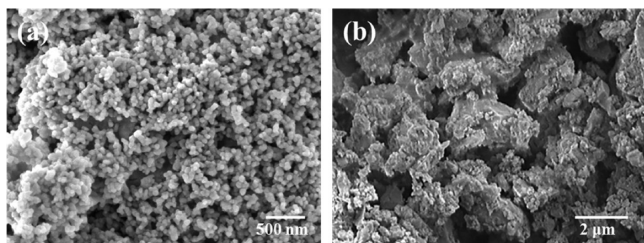
Figure 1. SEM micrographs of (a) ZrO_2 and (b) CaSi raw powders used in this study.

ZrO_2 spherical powders were composed of clusters of nanometer particles with a size of 40 nm, consistent with the manufacturer's data. In contrast, the average size of irregular CaSi particles was about 1 μm, as in the previous study.[31]

3.2. Phase Composition and Density of Sintered Sample. The XRD patterns of all sintered ZrO_2-CaSi samples including the CaSi powder are shown in Figure 2. The CaSi additive exhibited a relatively low intensity of major diffraction peaks at $2\theta = 32–34°$, which were assigned to the β-Ca_2SiO_4 (β-dicalcium silicate) phase.[28] Contrarily, the ZrO_2 control without CaSi (ZCS0) had a tetragonal zirconia (t-ZrO_2) phase consisting of $2\theta = 30.2, 34.6, 35.1, 50.1, 50.6,$ and $59.3°$, which were attributed to (101), (002), (110), (112), (200), and
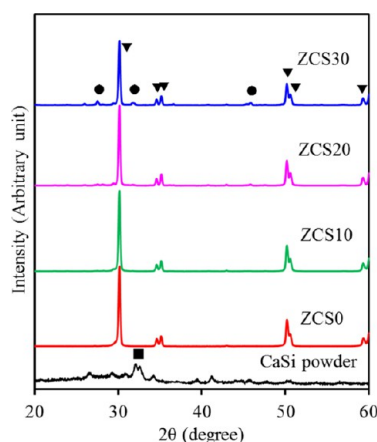
Figure 2. XRD patterns of the CaSi powder and various ZrO_2-CaSi composites. Notably, ZCS30 had the lower peak intensity than the other samples (triangle down solid: ZrO_2; box solid: β-Ca_2SiO_4; and circle solid: $CaZrO_3$ or $Ca_3ZrSi_2O_9$).

(103) crystal planes. When the CaSi powder was added to Y-TZP, the peak intensities of all t-ZrO_2 phases decreased with increasing CaSi content. Interestingly, for the 30% CaSi sample (ZCS30), new phases at $2\theta = 27.5, 31.8,$ and $45.8°$ appeared, which were possibly ascribed to $CaZrO_3$ and $Ca_3ZrSi_2O_9$,[37,38] in addition to the decrease in peak at $30.2°$. On the other hand, the apparent density of the ZCS0 control was 5.7 ± 0.2 g/cm^3 (Table 1), and the addition of increased CaSi content gradually decreased the density to $4.7 \pm 0.1, 4.1 \pm 0.1,$ and 3.9 ± 0.1 g/cm^3 for 10, 20, and 30 wt %, respectively, indicating a statistically significant difference ($p < 0.05$).

3.3. Mechanical Properties. *3.3.1. Three-Point Bending Strength and Modulus.* Table 1 lists the three-point bending strength and Young's modulus of various ZrO_2-based composites. With the increase in CaSi content, the strength and modulus of the samples decreased significantly ($p < 0.05$). The three-point bending strength of the ZrO_2 control was 486 MPa, which was significantly ($p < 0.05$) higher than those of all CaSi-containing composites. The 10 wt % CaSi-containing composite had a three-point bending strength value of 259 MPa, while 20 wt % CaSi resulted in a strength of 201 MPa. When 30 wt % CaSi was added to ZrO_2, the bending strength of the composite became 126 MPa. Regarding the modulus, ZCS10, ZCS20, and ZCS30 were 78, 48, and 20 GPa, respectively, which were significantly ($p < 0.05$) lower than the 128 GPa of the ZCS0 control.

3.3.2. Biaxial Strength. Table 1 also shows biaxial strength of the ZrO_2 control with and without CaSi, which revealed that the strength decreased significantly ($p < 0.05$) with increasing CaSi content. The biaxial strength of the control was 1164 MPa, while that of the composite containing 10 wt % CaSi became 631 MPa. The addition of 20 and 30 wt % CaSi to the ZrO_2 material produced biaxial strengths of 484 and 325 MPa, respectively.

3.3.3. Hardness. Vickers' microhardness value (Hv = 1406) of the ZCS0 control was significantly ($p < 0.05$) higher than those of all composites (Table 1). As the composites contained 10, 20, and 30 wt % CaSi, the resulting microhardness values were 1012, 708, and 622, respectively, which decreased significantly ($p < 0.05$) with increasing CaSi content. This was similar to the trend in the three-point bending strength and biaxial strength.

3.3.4. Fatigue. The results of fatigue are shown in $S-N$ diagrams (so-called fatigue life diagram), where S is the maximum stress in a cyclic loading and N is the number of cycles until fracture (Figure 3). The stability of all ZrO_2-based
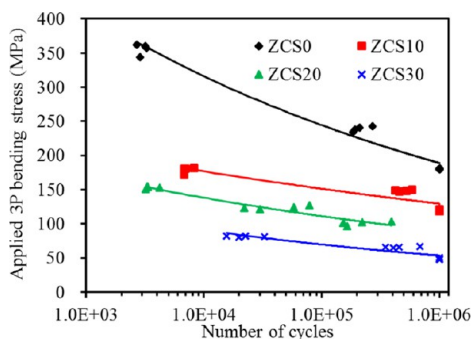
Figure 3. Fatigue curves of various samples under applied three-point bending stress versus the number of cycles to failure.

materials was noticeably affected by the cyclic loading, and as the number of cycles increased, the bending strength decreased remarkably. The ZrO_2 control (ZCS0) and ZCS10 were fatigued for 10^6 cycles, and their original three-point bending strengths were significantly reduced to approximately 37 and 55%, respectively. When subjected to a three-point bending stress of 100 MPa, the fatigued ZCS20 continued for approximately 2×10^5 cycles until failure occurred. For ZSC30, an applied stress of 80 MPa resulted in 3×10^4 failure cycles.

**3.4. In Vitro Degradation.** *3.4.1. Phase Composition.* The potential variations in material properties were worth verifying when long-term soaking in a physiological solution. After soaking in a dynamic SBF solution with pH 5.0, the XRD patterns of the ZrO_2 control did not exhibit obvious changes with increasing soaking time (Figure 4a). In contrast, the phase composition of all composites changed significantly during the 6 month soaking period (Figure 4b−d), especially for the ZCS20 and ZCS30 groups. In the case of ZCS30, in addition to the greatly reduced intensity of t-ZrO_2 phases and the disappearance of calcium zirconium silicate, new low-intensity peaks at 28.2 and 31.4° were also found, which were attributed to the monoclinic ZrO_2 (m-ZrO_2) phases of (−111) and (111), respectively. As the soaking time increased, the monoclinic phase became more remarkable.

3.4.2. Morphology. Broad-face SEM micrographs of the samples before soaking in SBF are shown in Figure 5. The ZrO_2 control (ZCS0) showed a highly dense body after sintering at 1350 °C and consisted of equiaxed grains with a size of about 100 nm. The presence of CaSi led to the formation of few micropores and increased the grain size to about 250 nm. After soaking in SBF for 1 month, the surface morphology of all samples changed with the appearance of numerous etching-induced nanopores, especially for samples with high CaSi content. In addition, the grain size of all soaked samples became larger than those of the as-prepared samples. The microstructures of the 3 month-soaked and 6 month-soaked samples were similar to those of the 1 month sample.

3.4.3. Composition Analysis. To understand the changes in the microstructure, the EDS results showed that the (Ca + Si)/(Zr + Ca + Si) weight ratios of ZCS10, ZCS20, and ZCS30 before soaking were 3.2 ± 0.4, 12.7 ± 3.9, and 18.2 ± 1.8, respectively (Figure 6). After soaking, the (Ca + Si)/(Zr + Ca + Si) ratio was significantly reduced. Interestingly, the (Ca +
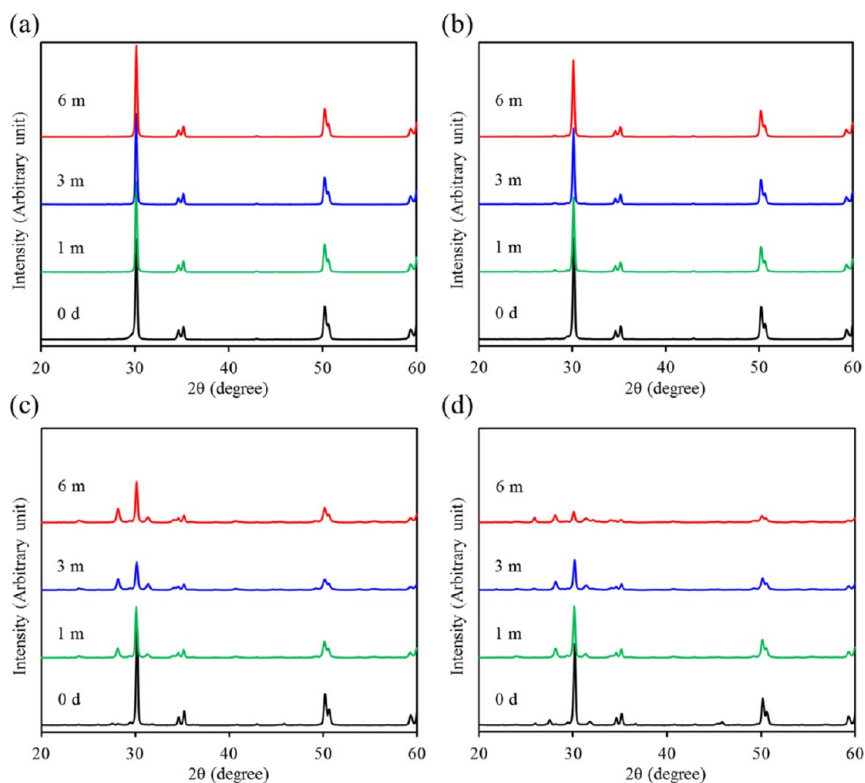
Figure 4. XRD patterns of various ZrO_2 samples containing (a) 0, (b) 10, (c) 20, and (d) 30 wt % CaSi before and after soaking in an SBF solution with pH 5 for predetermined time durations.
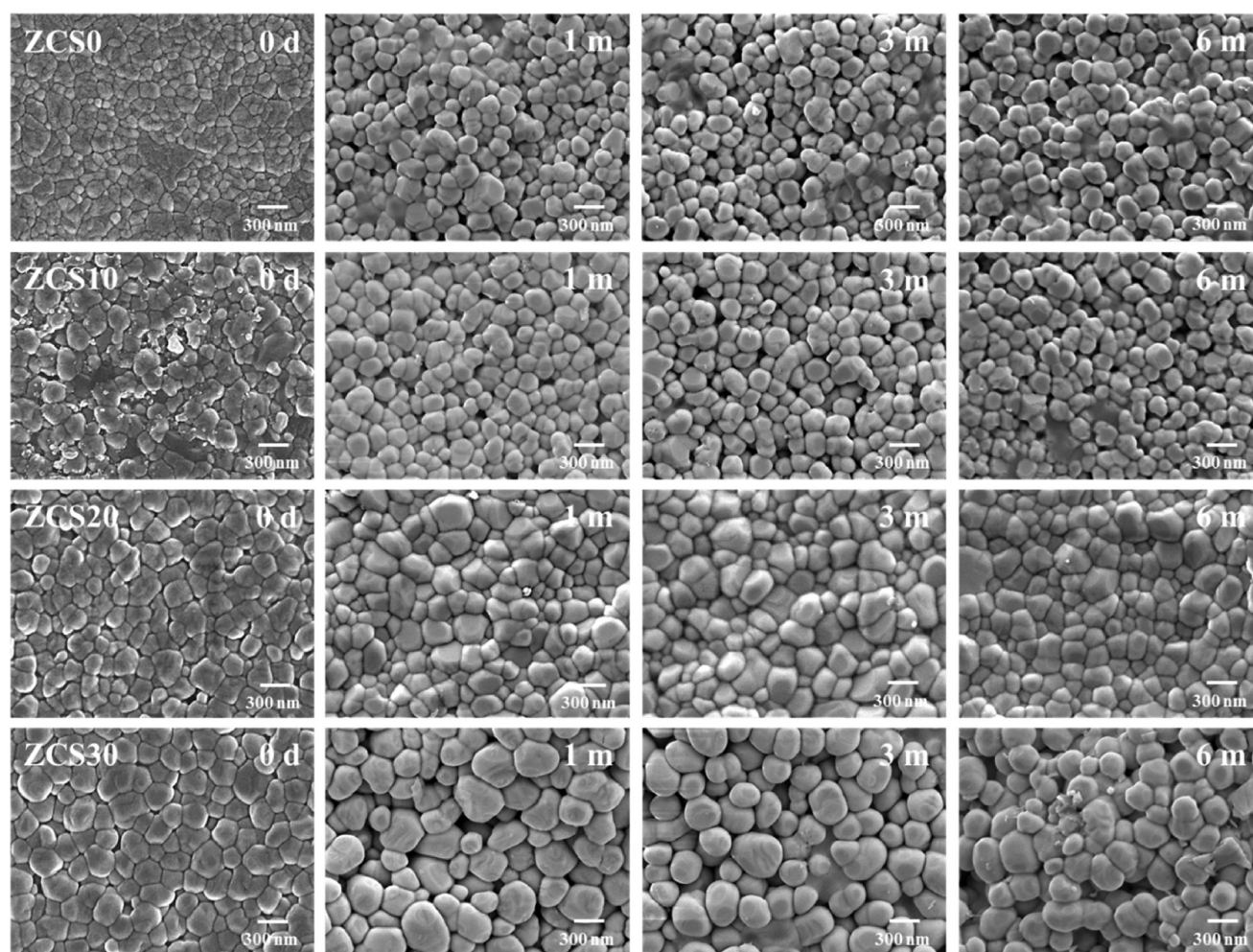
Figure 5. Surface SEM images of various ZrO_2-based materials before and after soaking in an SBF solution with pH 5 for 1, 3, and 6 months. The scale bars are 300 nm.

Si)/(Zr + Ca + Si) ratio of the composites with higher CaSi decreased more significantly. For example, in the sixth month, the ratio of ZCS10 was 2.1 ± 0.4 with a reduction of 34%, while ZCS30 had a ratio of 4.3 ± 1.2 with a reduction of 76%.

3.4.4. Biaxial Strength and Hardness. The changes in the biaxial strength of the materials as a function of soaking time are shown in Figure 7a. It can be clearly seen that the soaking time did not affect the biaxial strength of the ZCS0 control. One month of soaking did not cause the strength of all CaSi groups to decrease, whereas 3 month soaking made the biaxial strength of ZCS30 significantly lower ($p < 0.05$) than that of the as-prepared sample. However, after 6 months of soaking in pH 5.0 SBF, the biaxial strength of ZCS30 decreased by 52% reduction in terms of the original strength, while the biaxial strengths of ZCS10 and ZCS20 decreased by 16 and 29%, respectively. It is worthwhile to note that the biaxial strength of ZCS20 was 344 MPa, which was much higher than 155 MPa of ZCS30 after 6 month soaking. Regarding hardness, soaking time appeared to reduce the hardness of all samples. The hardness trends in CaSi groups were similar to the biaxial strength (Figure 7b). In comparison with the original hardness before soaking, the hardness of ZCS0, ZCS10, ZCS20, and ZCS30 decreased by 9, 19, 52, and 77%, respectively, after 6 months of a long-term soaking in pH 5.0 SBF.

3.4.5. Porosity and Weight Loss. The effect of soaking time on the porosity of the materials is shown in Figure 8a. The

original porosity values of all samples were less than 2%. After soaking for 1 month, the porosity of all samples increased to 2−5%. Not surprisingly, the higher the CaSi content, the greater the porosity revealed. After prolonged soaking for 6 months, the porosity remained between 2 and 6%. In the case of weight loss, the change depended on the type of sample (Figure 8b). ZrO_2 implants had almost no weight loss because of the large deviation, while the presence of CaSi caused an increase in weight loss. There was no significant difference ($p > 0.05$) between the samples soaked for 3 and 6 months. At the end of the 6 month soaking, the weight losses of ZCS0, ZCS10, ZCS20, and ZCS30 were 0.3, 0.7, 2.8, and 3.8%, respectively.

3.5. hMSC Responses. *3.5.1. Cell Growth.* The effect of CaSi contents in the composites on in vitro osteogenic activities of hMSCs was studied. The absorbance as a marker of the cell growth increased for all samples with increasing culture time (Figure 9). More importantly, the higher CaSi content in the composite resulted in a significantly ($p < 0.05$) greater cell growth at all culture time. After 7 days of culture, the growth of hMSCs seeded on ZCS30 was 74% higher than that of cells on the ZCS0 control.

3.5.2. ALP Activity. No matter which osteogenic induction medium (Figure 10a) or growth medium (Figure 10b) was used to culture hMSCs on the sample surface, the early cell differentiation activity consistently indicated that the compo-
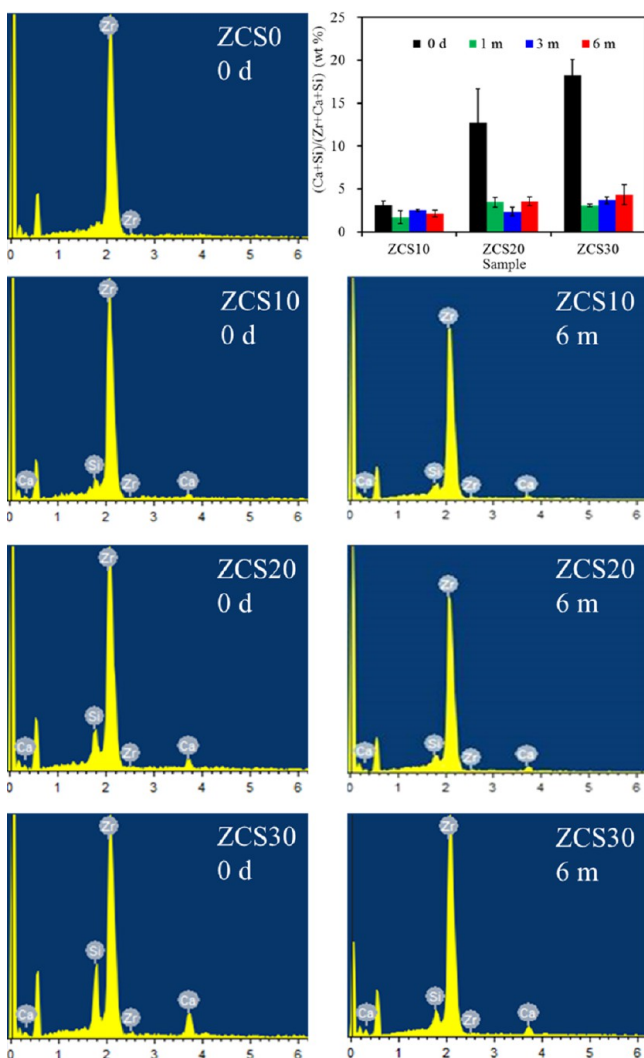
Figure 6. EDS profiles of various ZrO_2-based materials before and after soaking in SBF (pH 5.0) for 6 months. The changes in the (Ca + Si)/(Ca + Si + Zr) ratio by weight of various samples after soaking in SBF.

site material with higher CaSi content has significantly ($p < 0.05$) higher ALP expression. As an example, on day 14, the ALP of cells cultured on ZSC20 increased significantly ($p <$

0.05) by 31 and 26%, respectively, in the presence (Figure 10a) and the absence (Figure 10b) of osteogenic differentiation agents, compared with the ZCS0 control.

3.5.3. Mineralization. The low-magnification images of hMSCs stained with alizarin red S after 14 and 21 days of culture are shown in Figure 11. Remarkable differences can be found on the surfaces of the four samples. The hMSCs on the surface of the composites with higher CaSi content showed clearer mineralized matrix synthesis in the induction medium (Figure 11a) and growth medium (Figure 11b). It is clearly seen that when hMSCs were cultured in the growth medium without differentiation induction agents, lower calcium deposits were produced. After quantifying calcium deposits, regardless of the type of culture medium, the content of calcium deposits in ZCS0 was lower than that of the CaSi-containing samples. Not surprisingly, the samples with higher CaSi content were found to have greater mineral deposits, especially when cultured for 21 days. In the induction medium for 21 days (Figure 11a), the content of calcium deposits in ZCS20 samples was 1.8 times that of ZCS0 ($p < 0.05$), while the calcium deposits induced by cells in the growth medium were 1.4 times ($p < 0.05$) (Figure 11b).

3.6. Antibacterial Activity. *3.6.1. Bacterial Viability.* The higher CaSi content samples caused lower viability of *E. coli* bacteria than the lower CaSi content samples at all culture times (Figure 12a). For example, after bacterial seeding for 6 h, the 20% CaSi sample resulted in a viability of 23% for *E. coli*, indicating relatively effective antibacterial activity, while the viability of the ZCS0 control was 48%. On hour 48, the bacterial survival percentage on the surface of the 30% CaSi sample was about 51%, which was lower than the ZCS0 control (76%). In the case of *S. aureus*, a similar trend in the bacterial viability was also observed (Figure 12b), showing a clear CaSi content-dependent antibacterial ability of implants against *S. aureus*. As a result, the antibacterial ability of the 20% CaSi sample was about one times higher than that of the ZCS0 control throughout the culture period.

3.6.2. Bacterial Colony. To further clarify the antibacterial ability of the composite samples, bacterial colonies on the surfaces were observed by SEM. Compared to the ZCS0 control, the number of rod-shaped *E. coli* bacteria adhered to the CaSi samples was reduced (Figure 13). Similarly, the spherical Gram-positive *S. aureus* bacteria on the control aggregated into grape-like colonies, while few bacteria attached
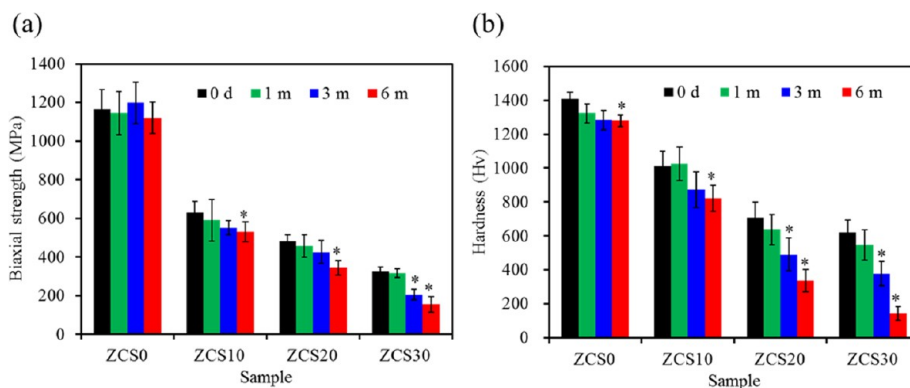

Figure 7. (a) Biaxial flexural strength and (b) hardness of various ZrO_2 samples containing different CaSi contents before and after soaking in an SBF solution with pH 5.0 for predetermined time durations. Asterisk represents a statistically significant difference ($p < 0.05$) from the corresponding as-prepared samples.
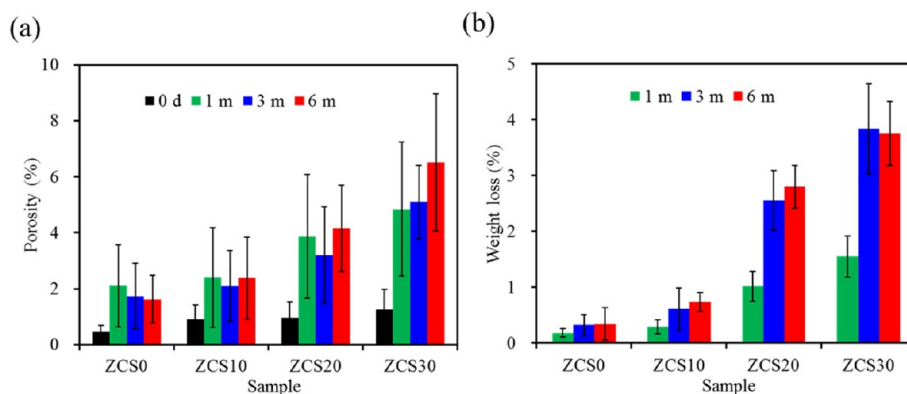
Figure 8. (a) Porosity and (b) weight loss of various ZrO_2 samples containing different CaSi contents after soaking in an SBF solution with pH 5.0 for predetermined time durations.
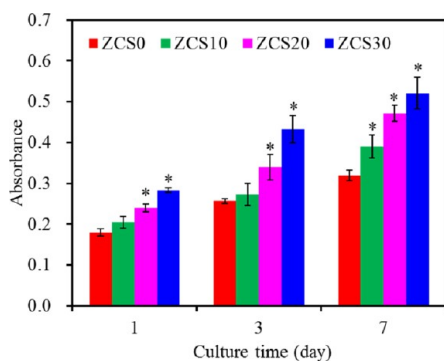
Figure 9. Cell growth of hMSCs cultured on the surfaces of various samples after various time points. Asterisk represents a statistically significant difference ($p < 0.05$) from the ZCS0 control.
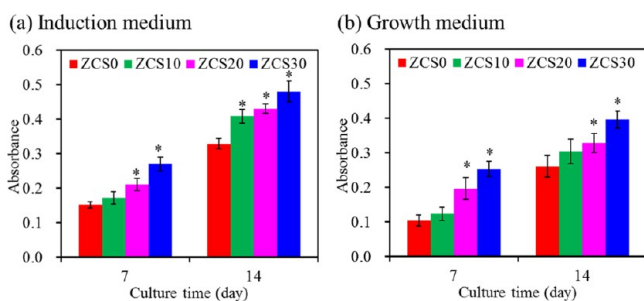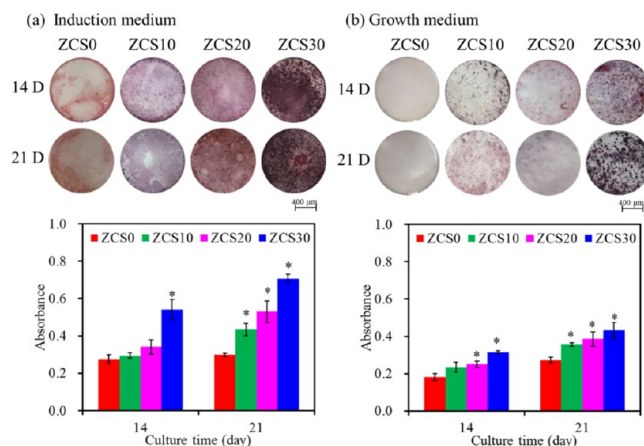

Figure 10. ALP activity of hMSCs on the surfaces of various samples after 7 and 14 days when cells were cultured in the growth medium (a) with and (b) without the differentiation induction agents. Asterisk represents a statistically significant difference ($p < 0.05$) from the ZCS0 control.
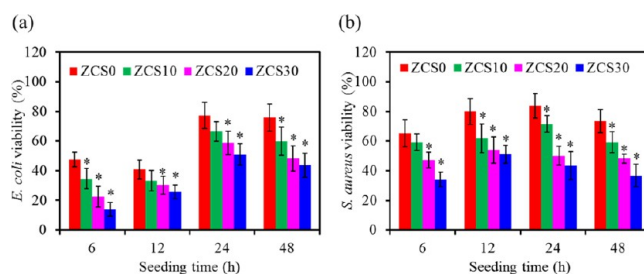

Figure 11. Photographs of hMSCs and the quantitative assay of the calcium deposit after staining with alizarin red S on the surfaces of various samples when cultured in the growth medium (a) with and (b) without the differentiation induction agents for 14 and 21 days. Asterisk represents a statistically significant difference ($p < 0.05$) from the ZCS0 control.

Figure 12. Viability of (a) *E. coli* and (b) *S. aureus* bacterial species cultured on the various sample surfaces for different time points. Viability is normalized to the control without materials. Asterisk represents a statistically significant difference ($p < 0.05$) from the ZCS0 control.

to the CaSi samples (Figure 14). The higher the CaSi content, the fewer the bacterial colonies were found on the sample.

4. DISCUSSION

The ideal load-bearing implant material should have the mechanical biocompatibility, excellent osteogenesis, and good antibacterial activity to match clinical needs. However, the stress-shielding effect and bacterial infections of load-bearing implants are the major obstacles to the dental and orthopedic applications. To this end, the purpose of this study was to harness highly bioactive calcium silicate with antibacterial efficacy to enhance biological properties and reduce the modulus of the high strength zirconia ceramics for prompting

the clinical success. First, the phase and morphology of the CaSi-ZrO_2 composite should be understood before unveiling mechanical biocompatibility. After sintering at 1350 °C, the addition of CaSi microparticles to the ZrO_2 nanoparticles did not cause the tetragonal−monoclinic phase transformation (t → m) of ZrO_2, and the t-ZrO_2 phase was the dominant phase for all samples. However, the diffusion reaction between Ca/Si and ZrO_2 promoted the formation of minor secondary phases,
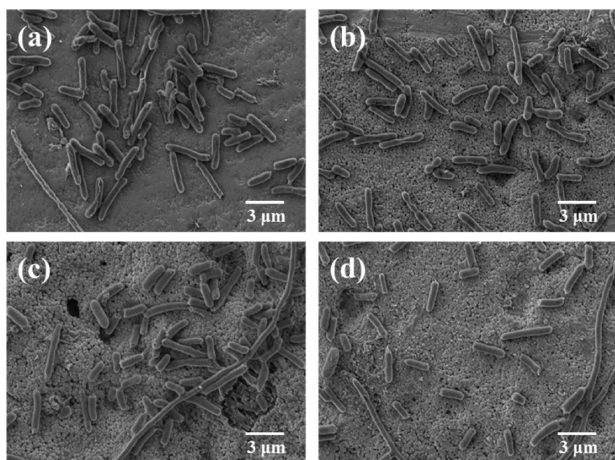
Figure 13. SEM micrographs of *E. coli* bacterial adhesion on the surfaces of (a) ZCS0 control, (b) ZCS10, (c) ZCS20, and (d) ZCS30 after 24 h of culture.
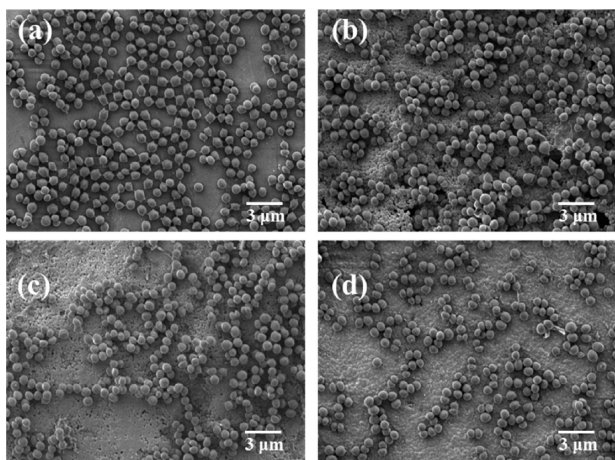
Figure 14. SEM micrographs of *S. aureus* bacterial adhesion on the surfaces of (a) ZCS0 control, (b) ZCS10, (c) ZCS20, and (d) ZCS30 after 24 h of culture.

such as calcium zirconium silicate and calcium zirconate. When doped with low percentages of CaO, MgO, and Y_2O_3 additives, the stabilization of t-ZrO_2 can be observed at high temperatures.[39] A previous study also indicates that the incorporation of $CaSiO_3$ into nano-ZrO_2 causes the phase transformation of m-ZrO_2 to t-ZrO_2.[40] Regarding density, it is not surprising that a lower CaSi density (about 2 g/cm^3) compared to ZrO_2 (6 g/cm^3)[41] may lead to a decrease in density. Indeed, when added to ZrO_2, 20 wt % CaSi (ZCS20) could generate a significant 28% reduction in density. Using CaSi to replace part of ZrO_2 with CaSi meant that there would be a great volume in the composite occupied by CaSi, which may affect mechanical properties and biological functions, as described below. The low density of the CaSi-containing composites, because they were close to bone density (2 g/cm^3),[42] may be advantageous to clinical use.

The load-bearing implant system should first meet general requirements, such as adequate mechanical properties, especially mechanical compatibility to avoid stress shielding. It is well recognized that high strength ZrO_2 has a much higher elastic modulus than the cortical bone. The mechanical properties of materials are closely related to their chemical composition, microstructure, process, and heat treatment. It is

reasonable that the optimization of the material composition may tailor the mechanical properties of the prepared material to make it equivalent to the mechanical properties of the natural bone by means of the composite approach due to the secondary phases. Therefore, it is important to optimize the composition of the CaSi-containing implants in order to eventually match the mechanical biocompatibility. This study indicated that the mechanical properties of composite samples decreased remarkably with increasing CaSi content. This reduction may be due to the inherent low mechanical strength and Young's modulus of the CaSi component, which acted almost like a structure softener in the ZrO_2 matrix. In addition, greater grain sizes in CaSi-containing composites may lead to lower mechanical properties. Kong et al. found that the addition of HA to ZrO_2–Al_2O_3 ceramic could enhance biocompatibility but would reduce the four-point bending strength.[43] Nevertheless, the three-point bending strengths of all ZrO_2-CaSi composite samples were in the range of 126–259 MPa, which was not less than the reported bending strength of the cortical bone (bending strength: 50–150 MPa).[14]

The mechanical features of load-bearing materials are fundamental to reach a balanced biomechanical load distribution at the bone–implant interface, which can reduce mechanical mismatch and facilitate the osteointegration process.[44] In addition to the requirement of adequate mechanical strength such as three-point bending strength and biaxial strength, the ideal elastic modulus of the implant materials should be close to that of the cortical bone being replaced. Given that the elastic modulus (200 GPa) of commercially available ZrO_2 products is much higher than that of the cortical bone (7–30 GPa),[14] this disparity gives rise to complications in mechanical biocompatibility between the ZrO_2 implant and bone tissue,[13,45] which can cause stress concentrations within the surrounding bone tissue and lead to bone resorption.[46] For this reason, the development of microporous materials or composite materials will reduce the elastic modulus of the ZrO_2 implant. Indeed, the incorporation of CaSi significantly reduced the modulus of the ZrO_2 control, undergoing from 128 GPa (the control) down to 20 GPa (ZCS30). This can be explained by the fact that the CaSi additive was not stiffer than the surrounding ZrO_2 ceramic matrix. Therefore, the modulus (20 to 78 MPa) of the composite implants decreased with increasing CaSi content, and these values were close to the cortical bone (7–30 GPa), enamel (80 GPa), and dentin (19 GPa).[46] The moduli of ZCS20 (48 MPa) and ZCS30 (20 MPa) were more conducive to reducing the "stress-shielding" effect and promoting the osseointegration. Piotrowski et al. adopted 3D finite element models to analyze the behavior of the bone–dental implant system depending on the elastic properties of the implant and found that the low modulus implant induced a stress distribution closer to the actual physiological phenomenon.[47] Brizuela et al. also studied the effect of six dental implants of Ti-based alloy with different elastic moduli (53–113 GPa) on the percentage of bone–implant contact in a minipig model.[48] They pointed out that lower elastic modulus allowed a greater and more efficient transfer of the mechanical load to the bone, favoring the formation of a new bone around the dental implant.

Another important mechanical property is hardness that is commonly used to measure plastic deformation resistance. The hardness of trabecular and cortical bone lamellae in the human

femur measured by nanoindentation ranges from 0.234 to 0.760 GPa (equivalent to 23.4 and 77.5 Hv),[49] and the hardness of alveolar bone is close to this range.[50] Dall'Ara et al. have stated that the Vickers hardness of the human trabecular bone was between 33 and 45 Hv.[51] In terms of teeth, the average hardness of primary enamel is 498 Hv and the hardness of dentin is 94 Hv.[52] By contrast, the hardness value of the ZrO_2 control was 1406 Hv, which was consistent with the values given in the literature,[41] but much higher than those of teeth and bone tissue. When CaSi was added to ZrO_2, such a large decrease in the hardness (325−631 Hv) of the ceramic-based composites may be related to the soft feature of the CaSi material. The decrease in hardness of CaSi-containing materials was possibly due to an increase in grain size based on the Hall−Petch relationship.

For bone implants used to support load-bearing therapy, the necessary mechanical prerequisite is to maintain mechanical strength under continuous and alternating loads throughout the entire implantation time required for bone healing, even if they degrade due to in vivo hydrolysis.[35] Therefore, fatigue degradation measurement is an important method to check the durability of load-bearing biomaterials because of its cyclic nature of in vivo loading.[53] In brittle ceramic materials, cyclic loading causes the propagation of small cracks, which in turn promoting them to failure at relatively low stresses. It can be reasonably speculated that detrimental effects on ZrO_2-based materials can be seen in fatigue tests. Indeed, as the number of cycles increased, the strength of all fatigued groups decreased noticeably. In the light of mechanical properties mentioned above, the introduction of CaSi into the ZrO_2 matrix reduced the flexural strength, hardness, and elastic modulus. Although it had lower fatigue resistance compared to ZrO_2, the other mechanical properties of the CaSi-containing composites were similar to those of the human cortical bone. This highlighted that the mechanical properties of CaSi-ZrO_2 could be tailored to mimic those of human teeth and bone tissue, thereby avoiding stress shielding.

Since mechanical stability is a critical issue for the clinical success of load-bearing materials, the implant material should maintain long-term clinical survival that can be in service within the tissue environment for many years. However, the t-ZrO_2 phase of ZrO_2 ceramic spontaneously transforms to the m-ZrO_2 phase in the presence of water or water vapor (hydrothermal aging) without applied stress,[54,55] which can affect its mechanical properties and surface characteristics. It is deduced that the humid environment in human body might affect the performance of CaSi-ZrO_2 composites. In addition, the acidity of liquids or food substances in the mouth may cause dissolution of the ceramic material and result in surface changes and/or material weakening.[56] In clinical practice, because of local metabolic acidosis or tissue inflammation induced by bacteria,[35] the pH of the bone lesion environment may change from a neutral value of 7.4 to an acidic pH as low as 5.0. Furthermore, the absorption rate of materials depends on the physiological environment (i.e., pH) and the properties of the material (i.e., solubility). For example, chemical degradation with 40% HF at ambient temperature could significantly reduce the three-point bending strength and Vickers hardness of Y-TZP.[57] Egilmez et al. have found that three-point bending strength of ZrO_2 was significantly decreased after soaking in acetic acid at 80 °C for 7 days.[56] For this reason, it is important to perform a long-term degradation test at pH 5.0 SBF, thereby predicting in vivo

stability before the preclinical trials. As a result, the long-term soaking in a pH 5.0 SBF solution influenced the physicochemical and mechanical properties of the composite materials. The continuous impact of acidic water molecules in pH 5.0 SBF into the lattice sites of t-ZrO_2 caused the t → m phase transformation of the CaSi samples, as evidenced by XRD. The grain growth observed in the SEM morphologies was possibly due to the volume expansion caused by the t → m transformation after prolonged soaking. It has been reported that exposing t-ZrO_2 to 3 kPa of H_2O or immersing it in liquid water at 25 °C would lead to its extensive (−80%) transformation to m-ZrO_2, which is attributed to a decrease in the difference between the surface free energy of m-ZrO_2 and that of t-ZrO_2 caused by the water adsorption.[58]

In general, t-ZrO_2 phase stability can be improved by doping low percentages of CaO, MgO, Y_2O_3, and CeO_2. This is because the structural similarity of the doped oxides and ZrO_2 increases the lattice strain and/or crystal defects.[59] As for SiO_2, its lattice constrain promotes tetragonal stabilization of ZrO_2 due to the formation of Si−O−Zr bonds.[39] It is speculated that the release of lattice strain or crystal defects may lead to a subsequent increase in the t → m transformation. Like low-temperature degradation at 134 °C, long-term in vitro degradation in pH 5.0 SBF may be initiated by isolated surface grains. Between the grains, water is incorporated into the ZrO_2 lattice through dissolution of Zr−O−Zr bonds and filling of oxygen vacancies.[55] After 3 months of soaking in pH 5.0 SBF, the addition of the 30% CaSi to Y-TZP caused a significant reduction in biaxial strength, while the 20% CaSi dopant maintained the strength. The material degradation may begin at the surface layer of the material and grow into the bulk of the material,[60] which in turn remarkably affects the mechanical properties.

The changes on the surface layer and in the bulk of the soaked samples can be also stated by the weight loss and porosity. When soaked in a long-term dynamic SBF solution, the ZrO_2 control exhibited very much small ion release, which was consistent with in vivo results.[61] Regarding composite materials, the ZCS30 sample with the highest CaSi content had the greatest weight loss and porosity, which was due to the release of the soluble fractions (CaSi). However, it revealed a relatively small degree of weight loss of <4% and porosity of about 6% even after a 6 month soaking time in pH 5.0 SBF. Not surprisingly, the CaSi component can be preferably dissolved compared to the ZrO_2 matrix, which was also confirmed by EDS. It is worthwhile to note that ionic dissolution products of CaSi-based ceramics support the biomimetic microenvironment, which is conducive to the growth and differentiation of human orofacial bone mesenchymal stem cells.[62] Dreger et al. have reported that released components from CaSi-based materials may stimulate mineral deposition at the material−dentin interface and inside the dentinal tubules.[63] Among the CaSi-ZrO_2 composites, ZCS20 was superior to ZCS30 in term of mechanical properties and long-term stability in vitro.

If osseointegration does not occur in a certain period of time, it may result in improper bonding of the implants to the bone tissues and eventually lead to implant failure.[64] There is no doubt that the high osteogenesis of the implant material plays a vital role in long-term clinical success. The biological function of an implant is closely linked to the surface chemistry of the materials used. Monkey animal model experiments have confirmed that ZrO_2 implants have no negative effects on soft

and hard tissues, showing similar osseointegration to titanium implants.[65] Although ZrO_2 exhibits low toxicity, at the same time, it has no direct bone bonding properties or osteoconduction behavior.[3,66] Rahaman et al. designed a functionally graded bioactive glass coating on magnesia partially stabilized zirconia to improve the biocompatibility of Mg-ZrO_2.[66] Matsumoto et al. prepared a composite of ZrO_2 and hydroxyapatite, which not only has compressive strength similar to the cortical bone but also has high cellular and tissue affinity.[19]

It is well recognized that hMSCs can be induced to differentiate into osteoblasts when cultured under appropriate conditions.[67] In this study, to further elucidate the effect of the CaSi additive on osteogenic activity, cell growth, proliferation, differentiation, and mineralization of hMSCs cultured on various samples in the absence and presence of the osteogenic differentiation medium were performed. There were significant differences in hMSC osteogenic activity between the ZrO_2 control and the CaSi-ZrO_2 groups. Greater numbers of hMSCs grew on the CaSi-containing material surfaces than on the ZrO_2 control at all culture times. More importantly, CaSi showed a significantly positive impact on the ALP activity and mineralization, irrespective of the presence of osteogenic differentiation agents such as dexamethasone, β-glycerophosphate, and ascorbic acid in the culture medium. In addition, supplementing the culture medium with osteogenic differentiation agents can induce more effective differentiation of hMSCs. Since osteogenic differentiation agents could stimulate osteoblastic differentiation of hMSCs, to clarify the role of CaSi in osteogenic differentiation, a growth medium may be used to examine the effect. Indeed, the current results confirmed that the presence of CaSi in the composites may promote the osteogenic differentiation of hMSCs under the culture conditions without osteogenic differentiation agents, highlighting the importance of material compositions. Gough et al. have reported that human osteoblast cells cultured in dissolution products of CaSi-based bioactive glass without osteogenic differentiation agent showed positive staining with alizarin red.[68] Thus, tailoring material characteristics such as chemical composition and surface structure can affect cell−material interactions.[69] Overall, the enhanced differentiation and mineralization of hMSCs consistently confirmed that the CaSi component in the ZrO_2-based implants played a positive role in the in vitro osteogenesis process. Thus, it can be speculated that the CaSi-ZrO_2 composites may be beneficial for bone regeneration upon implantation.

The elimination or prevention of biomaterial-associated infections has become a crucial factor in the success of an implantation treatment. Despite CaSi has been shown to have superior osteogenesis and antibacterial ability,[26] it is necessary to study the antibacterial activity of CaSi-ZrO_2 biocomposites. The ZrO_2 surface had a bacteriostatic effect to a certain extent, consistent with a previous study,[70] but the current results justified the advanced antibacterial activity of the CaSi-ZrO_2 groups. Bacterial viability directly responds to the antibacterial activity of the material surface. The bacterial viability of E. coli and S. aureus cultured on the CaSi-containing samples was significantly lower than that on the ZrO_2 control at all culture time points. Further, bacterial viability was inversely correlated with the CaSi content in the CaSi-ZrO_2 groups, revealing the dose-dependent antibacterial activity. The current findings also corresponded to SEM observations, in which the number of rod-shaped E. coli and spherical S. aureus bacteria adherent to

the surfaces of CaSi composites was markedly reduced when compared to the ZrO_2 control surface. Although the exact mechanism of the antibacterial activity of CaSi-ZrO_2 composites was not fully understood, the bacteriostatic effects were possibly due to surface charge, roughness, and modulus,[71] which affected bacterial adhesion that was the first step of bacterial colonization. The high CaSi content in the ZrO_2-based composite implants not only caused a substantial reduction in bacterial growth but also favored cell growth. In systems such as CaSi-ZrO_2 implants, one of the threefold benefits was the creation of mechanical compatibility matching the mechanical properties of the cortical bone (Figure 15).
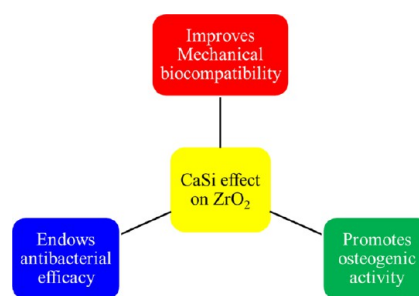
Figure 15. Schematic diagram showing the CaSi effect on characteristics of ZrO_2.

Another advantage was the use of a higher antimicrobial ability on the surface, which reduced the incidence of infection at the implantation site. The other was to offer a bioactive surface for osteoblast growth, thereby improving osteogenesis.

5. CONCLUSIONS

The development of mechanically compatible implant materials with enhanced osteogenic and antibacterial activities has drawn great interest. The incorporation of CaSi in ZrO_2 made the mechanical properties of the composites (including flexural strength, elastic modulus, and hardness) close to the cortical bone. Biological investigation confirmed that high CaSi content can effectively promote hMSC osteogenesis in vitro and inhibited bacterial growth. Taken together, ZrO_2 containing 20 wt % CaSi can be considered as a potential implant candidate in terms of mechanical compatibility, long-term stability, antibacterial ability, and osteogenic activity. The new CaSi-ZrO_2 biocomposite may be a promising candidate for load-bearing implants. To validate these potential bone implants, further research is needed, such as in vivo studies.

■ AUTHOR INFORMATION

Corresponding Author

Shinn-Jyh Ding − *Institute of Oral Science, Chung Shan Medical University, Taichung 402, Taiwan; Department of Stomatology, Chung Shan Medical University Hospital, Taichung 402, Taiwan;* orcid.org/0000-0002-2328-7126; Email: sjding@csmu.edu.tw

Authors

Ying-Hung Chu − *Institute of Oral Science, Chung Shan Medical University, Taichung 402, Taiwan*
Pei-Tung Chen − *Institute of Oral Science, Chung Shan Medical University, Taichung 402, Taiwan*

Complete contact information is available at:
https://pubs.acs.org/10.1021/acsomega.1c00097

Notes

The authors declare no competing financial interest.

■ REFERENCES

(1) Hench, L. L. Bioceramics: from concept to clinic. *J. Am. Ceram. Soc.* **1991**, *74*, 1487−1510.

(2) Piconi, C.; Maccauro, G. Zirconia as a ceramic biomaterial. *Biomaterials* **1999**, *20*, 1−25.

(3) Kelly, J. R. Dental ceramics: current thinking and trends. *Dent. Clin. North Am.* **2004**, *48*, 513−530.

(4) Hannouche, D.; Hamadouche, M.; Nizard, R.; Bizot, P.; Meunier, A.; Sedel, L. Ceramics in total hip replacement. *Clin. Orthop. Relat. Res.* **2005**, *430*, 62−71.

(5) Yan, M.; Csík, A.; Yang, C.-C.; Luo, Y.; Fodor, T.; Ding, S.-J. Synergistic reinforcement of surface modification on improving the bonding of veneering ceramics to zirconia. *Ceram. Int.* **2018**, *44*, 19665−19671.

(6) Yan, M.; Yang, C.-C.; Chen, Y.-H.; Ding, S.-J. Oxygen plasma improved shear strength of bonding between zirconia and composite resin. *Coatings* **2020**, *10*, 635.

(7) Covacci, V.; Bruzzese, N.; Maccauro, G.; Andreassi, C.; Ricci, G. A.; Piconi, C.; Marmo, E.; Burger, W.; Cittadini, A. In vitro evaluation of the mutagenic and carcinogenic power of high purity zirconia ceramic. *Biomaterials* **1999**, *20*, 371−376.

(8) Degidi, M.; Artese, L.; Scarano, A.; Perrotti, V.; Gehrke, P.; Piattelli, A. Inflammatory infiltrate, microvessel density, nitric oxide synthase expression, vascular endothelial growth factor expression, and proliferative activity in peri-implant soft tissues around titanium and zirconium oxide healing caps. *J. Periodontol.* **2006**, *77*, 73−80.

(9) Möller, B.; Terheyden, H.; Açil, Y.; Purcz, N. M.; Hertrampf, K.; Tabakov, A.; Behrens, E.; Wiltfang, J. A comparison of biocompatibility and osseointegration of ceramic and titanium implants: an in vivo and in vitro study. *Int. J. Oral Maxillofac. Surg.* **2012**, *41*, 638−645.

(10) Roehling, S.; Woelfler, H.; Hicklin, S.; Kniha, H.; Gahlert, M. A retrospective clinical study with regard to survival and success rates of zirconia implants up to and after 7 years of loading. *Clin. Implant Dent. Relat. Res.* **2016**, *18*, 545−558.

(11) Cho, Y.; Hong, J.; Ryoo, H.; Kim, D.; Park, J.; Han, J. Osteogenic responses to zirconia with hydroxyapatite coating by aerosol deposition. *J. Dent. Res.* **2015**, *94*, 491−499.

(12) Zhang, Y.; Jiang, F.; Luan, J.; Zhou, X.; Wu, Z.; Li, M.; Hong, Z. Surface properties of Ce-TZP/Al₂O₃ composite ceramics by coating mesoporous bioactive glass. *Composites, Part B* **2019**, *164*, 499−507.

(13) Sumner, D. R.; Gatahte, J. O. Determinants of stress shielding: design versus materials versus interface. *Clin. Orthop. Relat. Res.* **1992**, *274*, 202−205.

(14) Kokubo, T.; Kim, H. M.; Kawashita, M. Novel bioactive materials with different mechanical properties. *Biomaterials* **2003**, *24*, 2161−2175.

(15) Wei, C. K.; Ding, S. J. Dual-functional bone implants with antibacterial ability and osteogenic activity. *J. Mater. Chem. B* **2017**, *5*, 1943−1953.

(16) Kohal, R. J.; Knauf, M.; Larsson, B.; Sahlin, H.; Butz, F. One-piece zirconia oral implants: one-year results from a prospective cohort study. 1. Single tooth replacement. *J. Clin. Periodontol.* **2012**, *39*, 590−597.

(17) Geetha, M.; Singh, A. K.; Asokamani, R.; Gogia, A. K. Ti based biomaterials, the ultimate choice for orthopaedic implants − A review. *Prog. Mater. Sci.* **2009**, *54*, 397−425.

(18) Marchi, J.; Ussui, V.; Delfino, C. S.; Bressiani, A. H. A.; Marques, M. M. Analysis *in vitro* of the cytotoxicity of potential implant materials. I: zirconia−titania sintered ceramics. *J. Biomed. Mater. Res., B* **2010**, *94*, 305−311.

(19) Matsumoto, T. J.; An, S.-H.; Ishimoto, T.; Nakano, T.; Matsumoto, T.; Imazato, S. Zirconia−hydroxyapatite composite material with micro porous structure. *Dent. Mater.* **2011**, *27*, e205−e212.

(20) Abd El-Ghany, O. S.; Sherief, A. H. Zirconia based ceramics, some clinical and biological aspects: Review. *Future Dent. J.* **2016**, *2*, 55−64.

(21) Jo, J. K.; El-Fiqi, A.; Lee, J. H.; Kim, D. A.; Kim, H. W.; Lee, H. H. Rechargeable microbial anti-adhesive polymethyl methacrylate incorporating silver sulfadiazine-loaded mesoporous silica nano-carriers. *Dent. Mater.* **2017**, *33*, e361−e372.

(22) Egawa, M.; Miura, T.; Kato, T.; Saito, A.; Yoshinari, M. In vitro adherence of periodontopathic bacteria to zirconia and titanium surfaces. *Dent. Mater. J.* **2013**, *32*, 101−106.

(23) Persson, L. G.; Ericsson, I.; Berglundh, T.; Lindhe, J. Osseointegration following treatment of peri-implantitis and replacement of implant components. An experimental study in the dog. *J. Clin. Periodontol.* **2001**, *28*, 258−263.

(24) Huang, T. C.; Chen, C. J.; Chen, C. C.; Ding, S. J. Enhancing osteoblast functions on biofilm-contaminated titanium alloy by concentration-dependent use of methylene blue-mediated antimicrobial photodynamic therapy. *Photodiagn. Photodyn. Ther.* **2019**, *27*, 7−18.

(25) Zhang, N.; Molenda, J. A.; Fournelle, J. H.; Murphy, W. L.; Sahai, N. Effects of pseudowollastonite (CaSiO₃) bioceramic on in vitro activity of human mesenchymal stem cells. *Biomaterials* **2010**, *31*, 7653−7665.

(26) Huang, S. C.; Wu, B. C.; Ding, S. J. Stem cell differentiation-induced calcium silicate cement with bacteriostatic activity. *J. Mater. Chem. B* **2015**, *3*, 570−580.

(27) Xu, S.; Lin, K.; Wang, Z.; Chang, J.; Wang, L.; Lu, J.; Ning, C. Reconstruction of calvarial defect of rabbits using porous calcium silicate bioactive ceramics. *Biomaterials* **2008**, *29*, 2588−2596.

(28) Wu, I. T.; Kao, P. F.; Huang, Y. R.; Ding, S. J. In vitro and in vivo osteogenesis of gelatin-modified calcium silicate cement with washout resistance. *Mater. Sci. Eng. C* **2020**, *117*, 111297.

(29) Stowe, T. J.; Sedgley, C. M.; Stowe, B.; Fenno, J. C. The effects of chlorhexidine gluconate (0.12%) on the antimicrobial properties of tooth-colored ProRoot mineral trioxide aggregate. *J. Endod.* **2004**, *30*, 429−431.

(30) Wu, B. C.; Wei, C. K.; Hsueh, N. S.; Ding, S. J. Comparative cell attachment, cytotoxicity and antibacterial activity of radiopaque dicalcium silicate cement and white-coloured mineral trioxide aggregate. *Int. Endod. J.* **2015**, *48*, 268−276.

(31) Huang, Y. R.; Wu, I. T.; Chen, C. C.; Ding, S. J. In vitro comparisons of microscale and nanoscale calcium silicate particles. *J. Mater. Chem. B* **2020**, *8*, 6034−6047.

(32) Natale, L. C.; Rodrigues, M. C.; Xavier, T. A.; Simões, A.; de Souza, D. N.; Braga, R. R. Ion release and mechanical properties of calcium silicate and calcium hydroxide materials used for pulp capping. *Int. Endod. J.* **2015**, *48*, 89−94.

(33) Choi, B.-J.; Yoon, S.; Im, Y.-W.; Lee, J.-H.; Jung, H.-J.; Lee, H.-H. Uniaxial/biaxial flexure strengths and elastic properties of resin-composite block materials for CAD/CAM. *Dent. Mater.* **2019**, *35*, 389−401.

(34) Ding, S. J.; Chu, Y. H.; Wang, D. Y. Enhanced properties of novel zirconia-based osteo-implant systems. *Appl. Mater. Today* **2017**, *9*, 622−632.

(35) Wei, C. K.; Ding, S. J. Acid-resistant calcium silicate-based composite implants with high-strength as load-bearing bone graft substitutes and fracture fixation devices. *J. Mech. Behav. Biomed. Mater.* **2016**, *62*, 366−383.

(36) Lin, M. C.; Chen, C. C.; Wu, I. T.; Ding, S. J. Enhanced antibacterial activity of calcium silicate-based hybrid cements for bone repair. *Mater. Sci. Eng. C* **2020**, *110*, 110727.

(37) Ianoş, R.; Barvinschi, P. Solution combustion synthesis of calcium zirconate, CaZrO₃, powders. *J. Solid State Chem.* **2010**, *183*, 491−496.

(38) Schumacher, T. C.; Volkmann, E.; Yilmaz, R.; Wolf, A.; Treccani, L.; Rezwan, K. Mechanical evaluation of calcium-zirconium-silicate (baghdadite) obtained by a direct solid-state synthesis route. *J. Mech. Behav. Biomed. Mater.* **2014**, *34*, 294−301.

(39) del Monte, F.; Larsen, W.; Mackenzie, J. D. Chemical interactions promoting the ZrO₂ tetragonal stabilization in ZrO₂−SiO₂ binary oxides. *J. Am. Ceram. Soc.* **2000**, *83*, 1506−1512.

(40) Shuai, C.; Feng, P.; Yang, B.; Cao, Y.; Min, A.; Peng, S. Effect of nano-zirconia on the mechanical and biological properties of calcium silicate scaffolds. *Int. J. Appl. Ceram. Technol.* **2015**, *12*, 1148−1156.

(41) Kaplan, M.; Park, J.; Kim, S. Y.; Ozturk, A. Production and properties of tooth-colored yttria stabilized zirconia ceramics for dental applications. *Ceram. Int.* **2018**, *44*, 2413−2418.

(42) Phelps, J. B.; Hubbard, G. B.; Wang, X.; Agrawal, C. M. Microstructural heterogeneity and the fracture toughness of bone. *J. Biomed. Mater. Res.* **2000**, *51*, 735−741.

(43) Kong, Y.-M.; Bae, C.-J.; Lee, S.-H.; Kim, H.-W.; Kim, H.-E. Improvement in biocompatibility of ZrO₂−Al₂O₃ nano-composite by addition of HA. *Biomaterials* **2005**, *26*, 509−517.

(44) Sprio, S.; Tampieri, A.; Celotti, G.; Landi, E. Development of hydroxyapatite/calcium silicate composites addressed to the design of load-bearing bone scaffolds. *J. Mech. Behav. Biomed. Mater.* **2009**, *2*, 147−155.

(45) Murugan, R.; Ramakrishna, S. Development of nanocomposites for bone grafting. *Comp. Sci. Technol.* **2005**, *65*, 2385−2406.

(46) Dujovne, A. R.; Bobyn, J. D.; Krygier, J. J.; Miller, J. E.; Brooks, C. E. Mechanical compatibility of noncemented hip prostheses with the human femur. *J. Arthroplasty* **1993**, *8*, 7−22.

(47) Piotrowski, B.; Baptista, A. A.; Patoor, E.; Bravetti, P.; Eberhardt, A.; Laheurte, P. Interaction of bone−dental implant with new ultra low modulus alloy using a numerical approach. *Mater. Sci. Eng., C* **2014**, *38*, 151−160.

(48) Brizuela, A.; Herrero-Climent, M.; Rios-Carrasco, E.; Rios-Santos, J. V.; Pérez, R. A.; Manero, J. M.; Mur, J. G. Influence of the elastic modulus on the osseointegration of dental implants. *Materials* **2019**, *12*, 980.

(49) Zysset, P. K.; Guo, X. E.; Hoffler, C. E.; Moore, K. E.; Goldstein, S. A. Elastic modulus and hardness of cortical and trabecular bone lamellae measured by nanoindentation in the human femur. *J. Biomech.* **1999**, *32*, 1005−1012.

(50) Chang, M. C.; Ko, C. C.; Liu, C. C.; Douglas, W. H.; DeLong, R.; Seong, W.-J.; Hodges, J.; An, K.-N. Elasticity of alveolar bone near dental implant−bone interfaces after one month's healing. *J. Biomech.* **2003**, *36*, 1209−1214.

(51) Dall'Ara, E.; Öhman, C.; Baleani, M.; Viceconti, M. The effect of tissue condition and applied load on Vickers hardness of human trabecular bone. *J. Biomech.* **2007**, *40*, 3267−3270.

(52) Mahoney, E.; Holt, A.; Swain, M.; Kilpatrick, N. The hardness and modulus of elasticity of primary molar teeth: an ultra-micro-indentation study. *J. Dent.* **2000**, *28*, 589−594.

(53) Carter, D. R.; Caler, W. E.; Spengler, D. M.; Frankel, V. H. Uniaxial fatigue of human cortical bone. The influence of tissue physical characteristics. *J. Biomech.* **1981**, *14*, 461−470.

(54) Pereira, G. K. R.; Venturini, A. B.; Silvestri, T.; Dapieve, K. S.; Montagner, A. F.; Soares, F. Z. M.; Valandro, L. F. Low-temperature degradation of Y-TZP ceramics: A systematic review and meta-analysis. *J. Mech. Behav. Biomed. Mater.* **2016**, *55*, 151−163.

(55) Guo, X. Property degradation of tetragonal zirconia induced by low-temperature defect reaction with water molecules. *Chem. Mater.* **2004**, *16*, 3988−3994.

(56) Egilmez, F.; Ergun, G.; Cekic-Nagas, I.; Vallittu, P. K.; Lassila, L. V. J. Factors affecting the mechanical behavior of Y-TZP. *J. Mech. Behav. Biomed. Mater.* **2014**, *37*, 78−87.

(57) Xie, H.; Shen, S.; Qian, M.; Zhang, F.; Chen, C.; Tay, F. R. Effects of acid treatment on dental zirconia: an in vitro study. *PLoS One* **2015**, *10*, No. e0136263.

(58) Xie, S.; Iglesia, E.; Bell, A. T. Water-Assisted tetragonal-to-monoclinic phase transformation of ZrO₂ at low temperatures. *Chem. Mater.* **2000**, *12*, 2442−2447.

(59) del Monte, F.; Larsen, W.; Mackenzie, J. D. Stabilization of tetragonal ZrO₂ in ZrO₂−SiO₂ binary oxides. *J. Am. Ceram. Soc.* **2000**, *83*, 628−634.

(60) Amat, N. F.; Muchtar, A.; Amril, M. S.; Ghazali, M. J.; Yahaya, N. Effect of sintering temperature on the aging resistance and mechanical properties of monolithic zirconia. *J. Mater. Res. Technol.* **2019**, *8*, 1092−1101.

(61) Ichikawa, Y.; Akagawa, Y.; Nikai, H.; Tsuru, H. Tissue compatibility and stability of a new zirconia ceramic in vivo. *J. Prosthet. Dent.* **1992**, *68*, 322−326.

(62) Gandolfi, M. G.; Shah, S. N.; Feng, R.; Prati, C.; Akintoye, S. O. Biomimetic calcium-silicate cements support differentiation of human orofacial Mesenchymal Stem cells. *J. Endod.* **2011**, *37*, 1102−1108.

(63) Dreger, L. A. S.; Felippe, W. T.; Reyes-Carmona, J. F.; Felippe, G. S.; Bortoluzzi, E. A.; Felippe, M. C. S. Mineral trioxide aggregate and Portland cement promote biomineralization in vivo. *J. Endod.* **2012**, *38*, 324−329.

(64) Chen, X.; Chen, G.; He, H.; Peng, C.; Zhang, T.; Ngan, P. Osseointegration and biomechanical properties of the onplant system. *Am. J. Orthod.* **2007**, *132*, 278.e1−278.e6.

(65) Kohal, R. J.; Weng, D.; Bächle, M.; Strub, J. R. Loaded custom-made zirconia and titanium implants show similar osseointegration: an animal experiment. *J. Periodontol.* **2004**, *75*, 1262−1268.

(66) Rahaman, M. N.; Li, Y.; Bal, B. S.; Huang, W. Functionally graded bioactive glass coating on magnesia partially stabilized zirconia (Mg-PSZ) for enhanced biocompatibility. *J. Mater. Sci. Mater. Med.* **2008**, *19*, 2325−2333.

(67) Pittenger, M. F.; Mackay, A. M.; Beck, S. C.; Jaiswal, R. K.; Douglas, R.; Mosca, J. D.; Moorman, M. A.; Simonetti, D. W.; Craig, S.; Marshak, D. R. Multilineage potential of adult human mesenchymal stem cells. *Science* **1999**, *284*, 143−147.

(68) Gough, J. E.; Jones, J. R.; Hench, L. L. Nodule formation and mineralisation of human primary osteoblasts cultured on a porous bioactive glass scaffold. *Biomaterials* **2004**, *25*, 2039−2046.

(69) Yuan, H.; Fernandes, H.; Habibovic, P.; de Boer, J.; Barradas, A. M. C.; de Ruiter, A.; Walsh, W. R.; van Blitterswijk, C. A.; de Bruijna, J. D. Osteoinductive ceramics as a synthetic alternative to autologous bone grafting. *Proc. Natl. Acad. Sci. U. S. A.* **2010**, *107*, 13614−13619.

(70) Scarano, A.; Piattelli, M.; Caputi, S.; Favero, G. A.; Piattelli, A. Bacterial adhesion on commercially pure titanium and zirconium oxide disks: an in vivo human study. *J. Periodontol.* **2004**, *75*, 292−296.

(71) Song, F.; Koo, H.; Ren, D. Effects of material properties on bacterial adhesion and biofilm formation. *J. Dent. Res.* **2015**, *94*, 1027−1034.